Hindawi
Journal of Chemistry
Volume 2022, Article ID 9384592, 7 pages
https://doi.org/10.1155/2022/9384592

Research Article

Growth Kinetics of Zinc Sulphide Nanocrystals Synthesized by Colloidal Thermolysis of Fatty Acid Carboxylates

Michael. B. Mensah, Nathaniel O. Boadi, and Johannes A. M. Awudza

Department of Chemistry, Kwame Nkrumah University of Science and Technology, Private Mail Bag, Kumasi, Ghana

Correspondence should be addressed to Michael. B. Mensah; michael.mensah@knust.edu.gh

Received 9 June 2022; Accepted 26 July 2022; Published 27 August 2022

Academic Editor: Islam M. Al Akraa

Zinc sulphide (ZnS) is an important semiconductor with widespread electronic and catalytic applications. The growth kinetics of ZnS nanocrystals synthesized by the thermal decomposition of zinc ricinoleate carboxylates in an oleylamine:dodecanethiol (1 : 1) solvent mixture isreported. Crystalline sphalerite ZnS nanocrystals with quantum dot sizes of 2.3–5.3 nm were obtained at temperatures higher than 240°C. The p-XRD patterns showed a clear relationship between the crystallite sizes and the peak broadness at a temperature range of 250–300°C. The optical bandgap energies of the ZnS nanocrystals reduced from 4.27 eV to 3.73 eV as the time of reaction increased from 20 to 60 min at 250°C. The activation energy for the growth kinetics of the ZnS nanocrystals was determined to be 36.24 kJ/mol which compares closely to those reported in the literature for aqueous systems.

1. Introduction

Zinc sulphide is a direct wide bandgap (II-VI) semiconductor compound attractive for cathode-ray, catalytic, electroluminescence, solar cell, and UV laser applications [1–3]. It also has excellent optical properties in the infrared (IR) and the far-IR region [1, 4]. Thus, ZnS is a promising metal chalcogenide material that has attracted immense attention as a valuable transparent semiconductor for various electronic applications [5–9]. ZnS is a white to slightly yellowish material, and it is mostly considered an alternative to cadmium (Cd)-containing semiconductor chalcogenides (such as CdS, CdSe, and CdTe) because it is nontoxic and more suitable for biological applications [8, 10]. CdS, however, has been synthesized using a greener approach [11].

ZnS nanoparticles are usually obtained by reacting a zinc salt and sulphur using the coprecipitation method [12, 13]. Sulphur could be elemental sulphur or a sulphur-containing compound such as sodium sulphide, thiourea, cysteine, and dodecanethiol [5, 14, 15]. This method is based on the precipitation of the ions in an aqueous solution. The pH of the solution is critical to the precipitation to form the desired nanomaterial. The coprecipitation method is cheaper than the other conventional methods; however, it yields fewer crystalline nanoparticles with many defects [16].

ZnS nanoparticles have received considerable research on their growth kinetics because of their high structural symmetry, which enhances the probability of an oriented attachment growth mechanism [17]. When the size of a nanoparticle is reduced, the electronic band structure is modified due to the quantum confinement effect and results in an increment of the bandgap energy of the nanocrystal. Practically, this increment in bandgap energy is observed as a blue shift in the absorption spectrum of the nanocrystal. This provides an indication as to how to probe the kinetics of the growth of the nanocrystal in solution by simply monitoring the UV-Vis spectra. The time-dependent evolution of UV-Vis absorption spectra has been extensively used to study the kinetics of ZnS nanocrystals [17–19].

The Brus equation (1) gives a relationship between the bandgap energy (E_g) and the radius (r) of the nanocrystal based on the reduced mass approximation:

$$E_g = E_{g(nc)} - E_{g(\text{bulk})} = \frac{h^2}{8r^2}\left(\frac{1}{m_e^*} + \frac{1}{m_h^*}\right) - \frac{1.8e^2}{4\pi\varepsilon_o\varepsilon r}, \quad (1)$$

where ΔE_g is the difference between the bandgap energy of the nanocrystal $E_{g(nc)}$ and the bulk bandgap energy $E_{g\,(\mathrm{bulk})}$. The effective masses for the electrons and holes are m_e^* and m_h^*. The ε_o and ε is the permittivity of a vacuum and the dielectric constant of the material in question, respectively; h is the Planck's constant and r is the radius of the spherical nanocrystal. The first term in equation (1) represents the kinetic energy of the exciton and dominates when r is small. The second term in equation (1) is the Coulombic interaction of the electron and hole [20]. For ZnS, $E_{g\,(bulk)} = 3.6eV$ (some publications used 3.54 eV),$m_e^* = 0.34m_e$, $m_h^* = 0.23m_e$, and $\varepsilon = 8.76$ [20, 21].

Tiemann et al. [19] employed in-situ stopped-flow UV absorption spectroscopy to investigate the growth of ZnS nanoparticles in a supersaturated aqueous medium. Aqueous solutions of $ZnSO_4$ and Na_2S were injected simultaneously into an observation cell with pressure-driven syringes and the stopped-flow signal was triggered for data acquisition. This study concluded qualitatively that the growth of ZnS nanoparticles within 40 milliseconds is governed predominantly by the Ostwald ripening, though other mechanisms such as coalescence may also occur. Using a similar technique, Huang et al. [17] also investigated the role of oriented attachment of ZnS crystal growth kinetics in both aqueous and mercaptoethanol-water solutions. Using XRD, HRTEM, and kinetic modeling, they were able to conclude that in both systems, early crystal growth of ZnS nanocrystals occurs via a crystallographically specific oriented attachment resulting in different stacking orders and faults. However, at longer reaction times, the surface irregularities are removed via a diffusion-controlled growth mechanism, resulting in rounded particles with complex internal structures.

The thermal decomposition of metal carboxylates or metal fatty acid salts (MFASs) in suitable organic solvents has also become attractive for the synthesis of ZnS nanoparticles and other very important nanoparticles because of the following reasons: (i) it yields good quality crystalline nanoparticles, (ii) it is reproducible, (iii) it is attractive for large scale synthesis, and (iv) it creates the opportunity to employ different naturally existing fatty acids [22–25]. MFASs are polyvalent metal soaps, prepared either by (i) metathesis of sodium or potassium fatty acid salt with metal salts in aqueous or polar solvents, (ii) dissolution or fusion of metal oxides (or hydroxides, oxyhydroxides, hydrocarbonates, carbonates) in hot fatty acids, or (iii) direct reaction of metal with hot fatty acids [24]. Though the MFASs route produces very good quality monodispersed crystalline nanoparticles than the coprecipitation method, the kinetics of ZnS nanoparticle growth using this route has not been vividly studied. The study of nanocrystal growth is fundamental to understanding the manipulation of material properties to tailor them for a specific application. This work reports the growth kinetics of ZnS nanoparticles synthesized by the thermolysis of zinc (II) ricinoleate carboxylate complex.

2. Materials and Methods

2.1. Materials. Zinc acetate dihydrate (98%, Sigma-Aldrich), dodecanethiol (≤100%, Sigma-Aldrich), oleylamine (≤100%, Sigma-Aldrich), sodium hydroxide (≥97%, Fisher Scientific), hexane (≥97, Honeywell/Riedel Haen), toluene (99.7%, Sigma-Aldrich), ethanol (≥99.8%, Sigma-Aldrich), and acetone (≥99%, Honeywell/Riedel Haen) were all used without further purification. The ricinoleic acid was isolated from castor oil (Sigma-Aldrich) using a previously published method by Vaisman et al. [26] and used to prepare the zinc (II) ricinoleate complex (the TGA pattern is shown in Figure S1).

2.2. Methods

2.2.1. Syntheses of ZnS Nanoparticles. The ZnS nanoparticles were synthesized following the method previously published by Mensah et al. [24]. Zinc (II) ricinoleate complex (0.91 mmol and 0.6 g) was dissolved in a 1 : 1 solvent mixture of dodecanethiol (41.75 mmol and 10 ml) and oleylamine (30.39 mmol and 10 ml) in a three-necked flask under a nitrogen gas atmosphere. The reaction temperature was raised to 300°C and maintained for an hour. The resulting solution was cooled to room temperature to obtain a white precipitate of ZnS nanoparticles. The precipitate was washed with ethanol several times to remove the excess oleylamine and dodecanethiol. The ZnS nanoparticles were dispersed in toluene before analysis.

2.2.2. Kinetics of ZnS Nanoparticles. The kinetics of the growth of the ZnS in the oleylamine: dodecanethiol (1 : 1) solvent mixture was studied by withdrawing aliquot samples from the reaction flask at 0, 10, 20, 30, 40, 50, and 60 minute intervals and at different temperatures of 240, 250, 260, 270, 280, 290, and 300°C.

2.2.3. Characterization. The powder X-ray diffraction patterns were obtained with a Bruker D8 diffractometer using Cu-Kα radiation ($\lambda = 1.5418$ Å, 30 kV, 40 mA, 2θ range (10–70°), with a scan speed of 2.0 deg/min and a step size of 0.05. The absorption spectra were obtained using a UV-1800 Shimadzu UV spectrophotometer. A micrograph of ZnS nanoparticles synthesized at 300°C was obtained using a JEOL 1010 transmission electron microscope (TEM) with an accelerating voltage of 100 kV and equipped with a Megaview III camera and Soft Imaging Systems iTEM software. The nanoparticle sizes from the TEM image were analyzed using the ImageJ/Fiji software package.

3. Results and Discussion

3.1. Formation and Growth of ZnS Nanoparticles. The ZnS nanoparticles were formed by decomposing the $[Zn(Ra)_2]$ complex in a hot dodecanethiol:oleylamine (1 : 1) solvent mixture at reaction temperatures above 240°C. The thermal decomposition of transition metal carboxylates has been reported to occur via the cleavage of the M-OCOR and MO-COR bonds (where M is the metal ion) in the metal carboxylates to release radical species (as shown in the reaction scheme in Figure 1) [27]. In the presence of dodecanethiol, the generated radical species react with the sulphur (in dodecanethiol chemical structure) to form the ZnS nanoparticles (Figure 1).

The oleylamine used as a solvent is said to enhance the reactivity of the metal carboxylate precursor via aminolysis reaction, thereby lowering the reaction temperature for the metal sulphide formation [28]. Oleylamine is a primary amine that can act as an electron donor at high temperatures. Oleylamine controls nanoparticle morphology and crystallinity by exhibiting affinity to metals through its NH_2 functional group [29]. It was observed that at reaction temperatures below 240°C, there was no formation of crystalline ZnS nanoparticles. Instead, a white powdered substance was obtained at the lower temperatures and showed no X-ray diffraction, suggesting it was an amorphous material. The p-XRD did not detect the formation of zinc oxide in any of the synthesized samples, implying that the samples obtained above 240°C were pure ZnS nanoparticles.

3.2. p-XRD and TEM Analyses of ZnS Nanoparticles. The p-XRD pattern of the ZnS nanoparticles synthesized at 300°C is shown in Figure 2(a). A pure phase of ZnS was obtained. The diffraction pattern strongly corresponds to a face-centered cubic β-ZnS with sphalerite (Zinc blende) crystal structure (JCPDS 03-065-0309). The p-XRD pattern showed three distinct peaks at 2theta values of 28.55°, 47.54°, and 56.44°, matching the X-ray diffraction at hkl (111), (220), and (311) planes in ZnS. The lattice parameter calculated was approximately 5.4064 Å, which compares with 5.4060 Å for a standard ZnS (JCPDS 03-065-0309). The TEM image showing the morphology of the ZnS nanoparticles synthesized at 300°C is shown in Figure 2(b). From the TEM image, the average particle size of the ZnS nanoparticles was calculated to be 4.84 (± 1.56) nm, which agrees closely with the crystallite particle size of 5.3 nm calculated from the XRD pattern. The absorption spectrum and Tauc's plot of the ZnS nanoparticles synthesized at 300°C are shown in Figure S2.

3.3. Effect of Temperature on p-XRD Patterns of ZnS Nanoparticles. The p-XRD patterns of the ZnS nanoparticles synthesized at different temperatures (240–300°C) are shown in Figure 3. No ZnS crystal phase change was observed with increasing reaction temperature (within the chosen temperature range).

The diffraction pattern of the ZnS nanoparticles synthesized at 240°C appeared broadened compared to those synthesized at 300°C. This broadening of the diffraction peaks was observed to be decreasing as the reaction temperature was increased. Scherer reports the broadening of XRD diffraction peaks to be inversely proportional to the size of the crystallites [30]. The full-width-half-maximum (FWHM) of the diffraction peaks of the ZnS nanoparticles was reduced by 57% as the reaction temperature was increased from 240°C to 300°C. This observation agrees with the fact that the ZnS crystallite size increased with increasing reaction temperature. The crystallite sizes of the ZnS nanoparticles increased from 2.3 nm to 5.3 nm as the reaction temperature increased from 240°C to 300°C (The correlation between particle sizes determined by XRD and UV-Vis is shown in Figure S3). The percentage increment in the particle size was calculated to be 130% which corresponds to the 57% reduction in the FWHM of the diffraction peak (reflection at (111) plane) as the temperature was increased to 300°C. Comparatively, Huang et al. [17] obtained 2.0 nm and 2.4 nm particle sizes of ZnS nanoparticles synthesized via the hydrothermal method using water and mercaptoethanol-water as solvents, respectively.

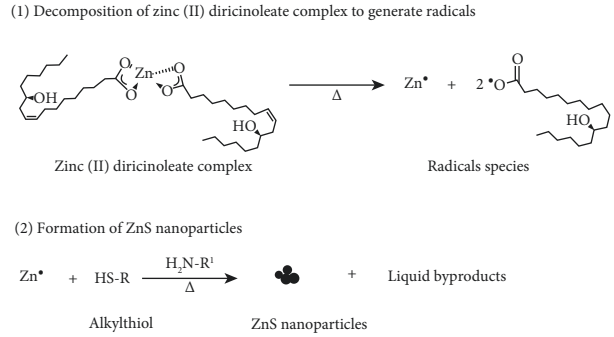

FIGURE 1: Reaction scheme showing the thermal decomposition of zinc (II), ricinoleate complex, and the formation of ZnS nanoparticles in dodecanethiol:oleylamine (1 : 1) solvent mixture at temperatures ≥240°C.

3.4. Effect of Reaction Time on the p-XRD Pattern of ZnS Nanoparticles. The p-XRD patterns of the ZnS nanoparticles synthesized at different time intervals at 270°C are shown in Figure 4. The crystallinity of the ZnS nanoparticles improved as the reaction progressed for a longer time (60 minutes). The material obtained at 10 minutes of reaction at 270°C showed no X-ray diffraction, indicating that the material was less crystalline. Increasing the reaction time to 60 minutes resulted in a comparatively more crystalline material.

The evolution of the optical spectra of the ZnS nanoparticles synthesized at different time intervals at 250°C is shown in Figure 5(a). The corresponding Tauc's plot estimation of the optical bandgap energies is also shown in Figure 5(b). The ZnS nanoparticles showed interesting time-dependent evolution of absorption spectra (Figure 5(a)). Good quality ZnS nanoparticles were obtained after the first 20 minutes of reaction at 250°C. The time-dependent absorption of ZnS nanoparticles has been employed by Tiemann et al. [19] and Li et al. [31] for the study of the coarsening kinetics of ZnS in aqueous systems.

The bandgap energy obtained for the ZnS nanoparticles synthesized at 250°C after the first 20 minutes of reaction was 4.27 eV and 3.73 eV after 60 min. This redshift of the optical spectra of the ZnS nanoparticles to a higher wavelength (or to lower energy) is due to the increase in the particle size with reaction time. This observation has been widely reported on ZnS nanoparticles and very important metal chalcogenide nanoparticles such as CdS and CdSe [31–37].

3.5. Activation Energy of ZnS Nanoparticle Growth. The coarsening kinetics of the ZnS nanoparticles in solution considering the Ostwald ripening and oriented attachment kinetic models is given by equation (2) [18, 38–40].

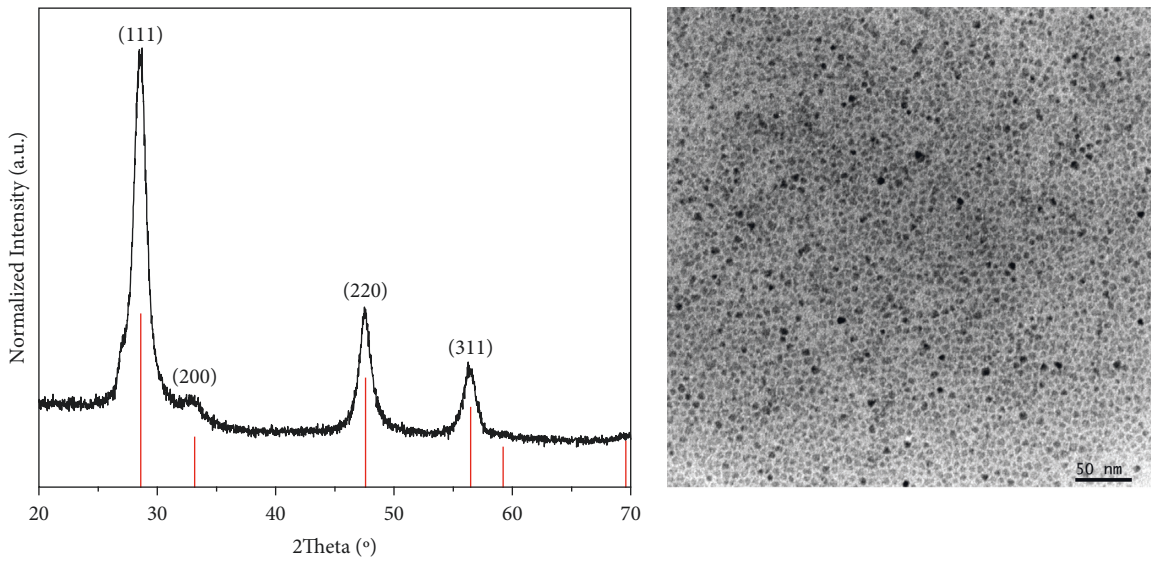

Figure 2: (a) The p-XRD pattern and (b) the TEM image of ZnS nanoparticles obtained by decomposing the zinc ricinoleate carboxylate complex in oleylamine: dodecanethiol (1 : 1) solvent mixture at 300°C for 1 hour. The red lines are the standard pattern for sphalerite ZnS (JCPDS 03-065-0309).

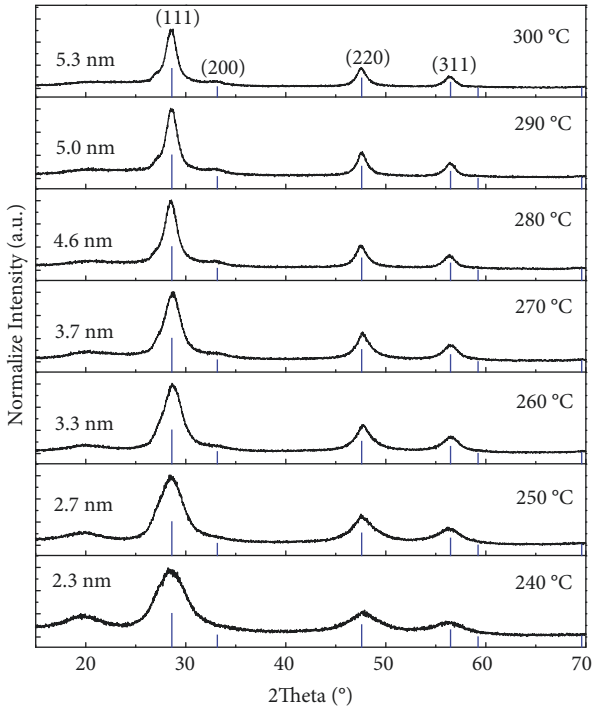

Figure 3: p-XRD patterns of ZnS nanoparticles obtained by decomposing ricinoleate carboxylate precursors in oleylamine: dodecanethiol (1 : 1) solvent mixtures at different temperatures for 1 hour. The blue lines are standard patterns for sphalerite ZnS (JCPDS 03-065-0309).

$$D = \frac{D_o\left(\sqrt[3]{2k_1 t} + 1\right)}{(k_1 t + 1)} + k_2 t^{1/n}, \tag{2}$$

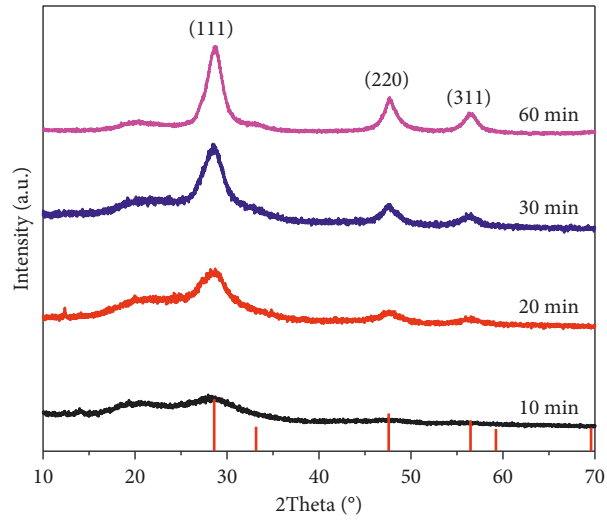

Figure 4: The effect of reaction time on p-XRD patterns of ZnS nanoparticles synthesized by the thermal decomposition of the zinc ricinoleate precursor in oleylamine/dodecanethiol (1 : 1) solvent mixture at 270°C.

where D is the particle diameter at time t, D_o is the initial particle diameter, and k_1 and k_2 are reaction rate constants for the two-step reaction in the crystal growth reaction. However, the growth component is the second term of equation (2) that dominates the coarsening activity over a longer period of a reaction than the first term, which diminishes rapidly in the reaction. Thus, k_2 dominates over k_1, and it is reported as the rate constant for ZnS nanoparticles' crystal growth. The plot of ZnS nanoparticles sizes against reaction time at different temperatures is shown in Figure 6.

At 280°C, the particle size increased rapidly during the first 30 to 40 minutes and stabilized afterwards. This suggests

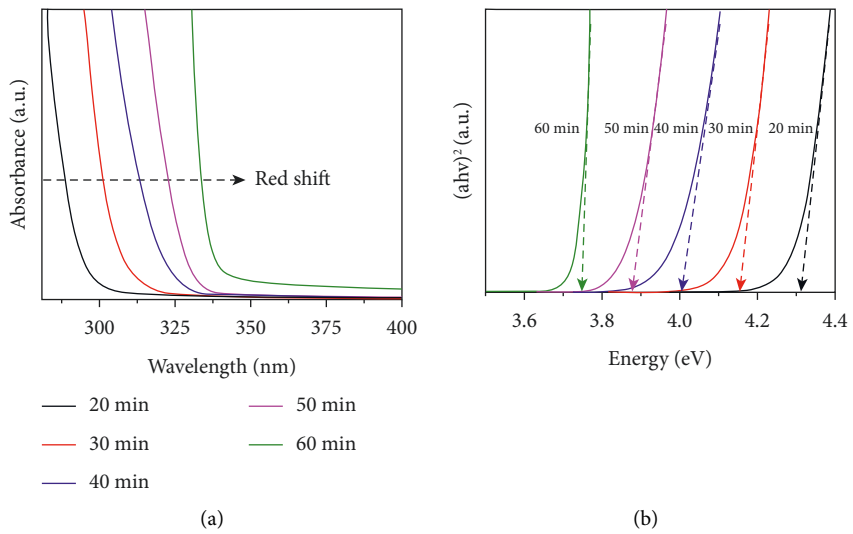

Figure 5: The effect of reaction time on (a) absorption spectra and (b) estimation of optical bandgap energy of ZnS nanoparticles synthesized by thermal decomposition of the zinc ricinoleate precursor in the oleylamine/dodecanethiol (1 : 1) solvent mixture at 250°C.

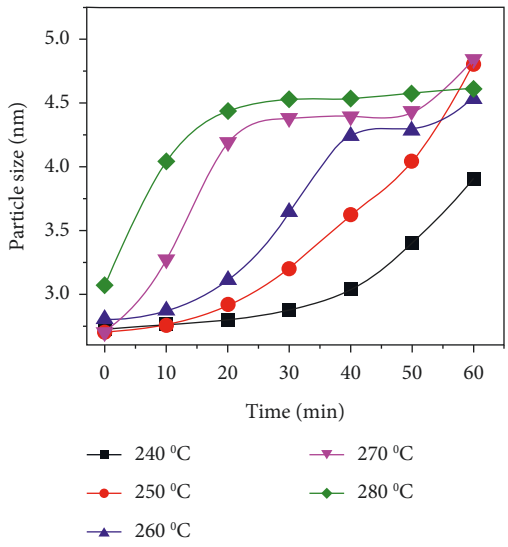

Figure 6: A plot of the average particle size of ZnS nanoparticles (obtained from UV-Vis spectra) against reaction time at different temperatures.

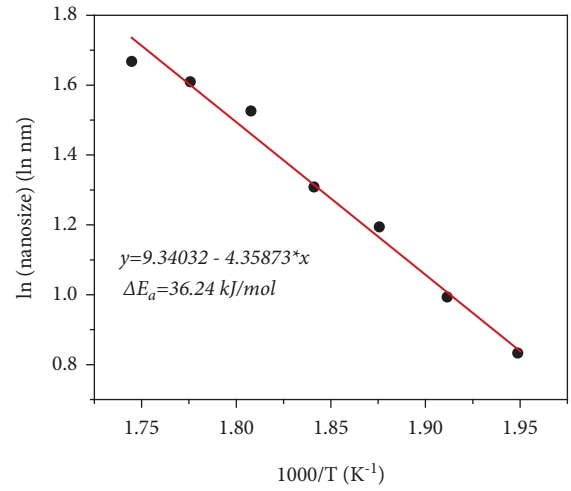

Figure 7: Arrhenius plot of in (D) against the reciprocal of temperature for ZnS nanocrystal growth in the oleylamine: dodecanethiol (1 : 1) solvent mixture. The nanocrystallite sizes were obtained from the XRD patterns at different reaction temperatures (Figure 3). (The correlation between particle sizes determined by XRD and UV-Vis is shown in Figure S3).

the possible size focusing mechanism occurs after the first 40 minutes of the reaction. During size focusing, according to the diffusion-controlled model, the larger particles grow slowly, whereas the smaller particles grow rapidly due to the large supply or diffusion of monomers/solutes to their surface. At 240°C and 250°C, the particle size grew gradually or slowly and at 260°C and 270°C the particle size increased rapidly and stabilized briefly and then increased rapidly again (Figure 6). The Ostwald ripening and oriented attachment mechanisms coexist for reactions at 240°C to 270°C. In the Ostwald ripening mechanism, the larger particles grow at the expense of the smaller particles. This is explained by assuming that the concentration of the solutes at the surfaces of the bigger particles is low compared to that of the smaller particles, and thus, solutes diffuse from the surfaces of the smaller particles to the bigger particles, resulting in the growth of the bigger particles. The oriented attachment mechanism assumes the coalescence of adjacent particles that share a common crystallographic orientation.

The activation energy (ΔE_a) of the coarsening reaction was calculated by employing the Arrhenius equation in the form reported by Kuo et al. [41].

$$\ln(D) = -\frac{\Delta E_a}{RT} + \ln(A), \tag{3}$$

where D is the nanocrystallite size (in nm), R is the ideal gas constant, T is the temperature in Kelvin, and A is the

preexponential factor. A plot of *ln (D)* against the reciprocal of the temperature is shown in Figure 7. The activation energy is calculated by multiplying the slope (obtained from the linear fit) and *R*. The ΔE_a value obtained for the growth of ZnS nanoparticles in a mixture of oleylamine and dodecanethiol (1 : 1) solvent mixture was 36.24 kJ/mol. This value agrees with the 42.4 kJ/mol reported by Huang et al. [17] for the coarsening of ZnS nanoparticles in an aqueous/mercaptoethanol medium. Tiemann et al. [18] also obtained ΔE_a of 25.7 kJ/mol for the coarsening of ZnS nanoparticles in an aqueous medium. The ΔE_a value obtained in this work considers all the possible crystal growth mechanisms accounted for in equation (2).

4. Conclusion

The thermal decomposition of zinc ricinoleate carboxylate complex in the oleylamine: dodecanethiol (1 : 1) solvent mixture shows the synthesis of ZnS nanoparticles. Pure crystalline sphalerite monodispersed ZnS nanoparticles with quantum dot sizes between 2.3 and 5.3 nm were obtained at temperatures higher than 240°C. The particle size and optical bandgap energy of the ZnS nanoparticles were found to be dependent on temperature and time of reaction. This synthesis route yielded clear time and temperature-dependent UV-Vis spectra and p-XRD patterns, valuable kinetics data. The activation energy for the nanocrystallite growth kinetics of ZnS nanoparticles in an oleylamine:dodecanethiol (1 : 1) solvent mixture was determined to be 36.24 kJ/mol.

Conflicts of Interest

The authors declare that they have no conflicts of interest.

Authors' Contributions

MBM designed the study, performed experiments, analyzed data, and drafted the manuscript. NOB and JAMA critically revised the manuscript for important intellectual content.

Acknowledgments

The authors wish to acknowledge the Leverhulme-Royal Society Africa Award-Postdoctoral Fellowship grants (LAF\R1\180018) and DFID-Royal Society Africa Capacity Building Initiative (ACBI) for providing financial support for this project. The Department of Chemistry, Kwame Nkrumah University of Science and Technology, Kumasi, is acknowledged for hosting the fellowship.

Supplementary Materials

Additional information on the thermogravimetric analysis of ricinoleate complex, UV-Vis spectrum ,and Tauc's plot, and the correlation between particle sizes of ZnS nanoparticles determined by XRD and UV-Vis spectroscopic methods. (*Supplementary Materials*)

References

[1] J. Han, W. Zhang, W. Chen, L. Thamizhmani, A. K. Azad, and Z. Zhu, "Far-infrared characteristics of ZnS nanoparticles measured by terahertz time-domain spectroscopy," *Journal of Physical Chemistry B*, vol. 110, no. 5, pp. 1989–1993, 2006.

[2] H. R. Azimi, M. Ghoranneviss, S. M. Elahi, M. R. Mahmoudian, F. Jamali-Sheini, and R. Yousefi, "Excellent photocatalytic performance under visible-light irradiation of ZnS/rGO nanocomposites synthesized by a green method," *Frontiers of Materials Science*, vol. 10, no. 4, pp. 385–393, 2016.

[3] H. R. Azimi, M. Ghoranneviss, S. M. Elahi, and R. Yousefi, "Photovoltaic and UV detector applications of ZnS/rGO nanocomposites synthesized by a green method," *Ceramics International*, vol. 42, no. 12, pp. 14094–14099, 2016.

[4] M. Afzaal, M. A. Malik, and P. O'Brien, "Preparation of zinc containing materials," *New Journal of Chemistry*, vol. 31, no. 12, pp. 2029–2040, 2007.

[5] W. He, H. Jia, J. Cai et al., "Production of reactive oxygen species and electrons from photoexcited ZnO and ZnS nanoparticles: a comparative study for unraveling their distinct photocatalytic activities," *Journal of Physical Chemistry C*, vol. 120, no. 6, pp. 3187–3195, 2016.

[6] J.-S. Hu, L.-L. Ren, Y.-G. Guo et al., "Mass production and high photocatalytic activity of ZnS nanoporous nanoparticles," *Angewandte Chemie*, vol. 117, no. 8, pp. 1295–1299, 2005.

[7] S. M. Ng, M. Koneswaran, and R. Narayanaswamy, "A review on fluorescent inorganic nanoparticles for optical sensing applications," *RSC Advances*, vol. 6, no. 26, pp. 21624–21661, 2016.

[8] M. Khalkhali, H. Zeng, Q. Liu, and H. Zhang, "Structural evolutions of ZnS nanoparticles in hydrated and bare states," *Journal of Physical Chemistry C*, vol. 120, no. 14, pp. 7870–7884, 2016.

[9] N. Kaur, S. Kaur, J. Singh, and M. Rawat, "A review on zinc sulphide nanoparticles: from synthesis, properties to applications," *Journal Bioelectron Nanotechnology*, vol. 1, no. 1, pp. 1–5, 2016.

[10] X. Fang, Y. Bando, U. K. Gautam et al., "ZnO and ZnS nanostructures: ultraviolet-light emitters, lasers, and sensors," *Critical Reviews in Solid State and Materials Sciences*, vol. 34, no. 3-4, pp. 190–223, 2009.

[11] M. B. Mensah, J. A. M. Awudza, N. Revaprasadu, and P. O'Brien, "Synthesis of CdS and PbS nanoparticles by the thermal decomposition of ethyl xanthate complexes in castor oil using the heat-up technique," *Materials Science in Semiconductor Processing*, vol. 122, pp. 105493–105498, 2021.

[12] Y. Zhang, X. Li, W. Xu, S. Li, H. Wang, and L. S. Li, "The size controlled synthesis and self-assembled of monodisperse Cu 2 S nanocrystals," *Materials Letters*, vol. 67, no. 1, pp. 117–120, 2012.

[13] J. Zhang, Z. Lin, Y. Lan et al., "A multistep oriented attachment kinetics: coarsening of ZnS nanoparticle in concentrated NaOH," *Journal of the American Chemical Society*, vol. 128, no. 39, pp. 12981–12987, 2006.

[14] C. M. Goodell, B. Gilbert, S. J. Weigand, and J. F. Banfield, "Kinetics of water adsorption-driven structural transformation of ZnS nanoparticles," *Journal of Physical Chemistry C*, vol. 112, no. 13, pp. 4791–4796, 2008.

[15] A. K. Kole, C. S. Tiwary, and P. Kumbhakar, "Morphology controlled synthesis of wurtzite ZnS nanostructures through simple hydrothermal method and observation of white light

emission from ZnO obtained by annealing the synthesized ZnS nanostructures," *Journal of Materials Chemistry C: Materials for Optical and Electronic Devices*, vol. 2, pp. 1–9, 2014.

[16] P. Wu and X.-P. Yan, "Doped quantum dots for chemo/biosensing and bioimaging," *Chemical Society Reviews*, vol. 42, no. 12, pp. 5489–5533, 2013.

[17] F. Huang, H. Zhang, and J. F. Banfield, "Two-stage crystal-growth kinetics observed during hydrothermal coarsening of nanocrystalline ZnS," *Nano Letters*, vol. 3, no. 3, pp. 373–378, 2003.

[18] M. Tiemann, F. Marlow, J. Hartikainen, O. Weiss, and M. Linden, "Ripening effects in ZnS nanoparticle growth," *Journal of Physical Chemistry C*, vol. 112, no. 5, pp. 1463–1467, 2008.

[19] M. Tiemann, Ö Weiß, J. Hartikainen, F. Marlow, and M. Linden, "Early stages of ZnS nanoparticle growth studied by in-situ stopped-flow UV absorption spectroscopy," *ChemPhysChem*, vol. 6, no. 10, pp. 2113–2119, 2005.

[20] R. Krsmanović Whiffen, D. Jovanović, Ž Antic et al., "Structural, optical and crystal field analyses of undoped and Mn^{2+}-doped ZnS nanoparticles synthesized via reverse micelle route," *Journal of Luminescence*, vol. 146, pp. 133–140, 2014.

[21] J. F. Suyver, S. F. Wuister, J. J. Kelly, and A. Meijerink, "Synthesis and photoluminescence of nanocrystalline ZnS: Mn^{2+}," *Nano Letters*, vol. 1, no. 8, pp. 429–433, 2001.

[22] S.-H. Choi, K. An, E.-G. Kim, J. H. Yu, J. H. Kim, and T. Hyeon, "Simple and generalized synthesis of semiconducting metal sulfide nanocrystals," *Advanced Functional Materials*, vol. 19, no. 10, pp. 1645–1649, 2009.

[23] J. D. Patel, F. Mighri, and A. Ajji, "Generalized chemical route to develop fatty acid capped highly dispersed semiconducting metal sulphide nanocrystals," *Materials Research Bulletin*, vol. 47, no. 8, pp. 2016–2021, 2012.

[24] M. B. Mensah, P. D. McNaughter, S. G. McAdams et al., "Ricinoleic acid as a green alternative to oleic acid in the synthesis of doped nanocrystals," *ChemistrySelect*, vol. 3, no. 48, pp. 13548–13552, 2018.

[25] M. B. Mensah, J. A. M. Awudza, and P. O'Brien, "Castor oil: a suitable green source of capping agent for nanoparticle syntheses and facile surface functionalization," *Royal Society Open Science*, vol. 5, no. 8, pp. 180824–180919, 2018.

[26] B. Vaisman, A. Shikanov, and A. J. Domb, "The isolation of ricinoleic acid from Castor oil by salt-solubility-based fractionation for the biopharmaceutical applications," *Journal of the American Oil Chemists' Society*, vol. 85, no. 2, pp. 169–184, 2008.

[27] H. G. Cha, D. K. Lee, Y. H. Kim, C. W. Kim, C. S. Lee, and Y. S. Kang, "Solventless nanoparticles synthesis under low pressure," *Inorganic Chemistry*, vol. 47, no. 1, pp. 121–127, 2007.

[28] J. Liu, H. Yu, Z. Wu, W. Wang, J. Peng, and Y. Cao, "Size-tunable near-infrared PbS nanoparticles synthesized from lead carboxylate and sulfur with oleylamine as stabilizer," *Nanotechnology*, vol. 19, no. 34, pp. 345602–345609, 2008.

[29] S. Mourdikoudis and L. M. Liz-Marza, "Oleylamine in nanoparticle synthesis," *Chemistry of Materials*, vol. 25, 2013.

[30] U. Holzwarth and N. Gibson, "The scherrer equation versus the debye–scherrer equation," *Nature Nanotechnology*, vol. 6, no. 9, p. 534, 2011.

[31] Z. Li, J. Wang, X. Xu, and X. Ye, "The evolution of optical properties during hydrothermal coarsening of ZnS nanoparticles," *Materials Letters*, vol. 62, no. 23, pp. 3862–3864, 2008.

[32] H. Su, J. D. Dixon, A. Y. Wang, J. Low, J. Xu, and J. Wang, "Study on growth kinetics of CdSe nanocrystals with a new model," *Nanoscale Research Letters*, vol. 5, pp. 823–828, 2010.

[33] M. Sun, H. Yu, W. Yang, L. Qi, F. Yang, and X. Yang, "Shape evolution of CdSe nanocrystals in vegetable oils: a synergistic effect of selenium precursor," *Colloids and Surfaces A: Physicochemical and Engineering Aspects*, vol. 350, no. 1–3, pp. 91–100, 2009.

[34] J. Zhang, F. Huang, and Z. Lin, "Progress of nanocrystalline growth kinetics based on oriented attachment," *Nanoscale*, vol. 2, no. 1, pp. 18–34, 2010.

[35] G. G. Yordanov, G. D. Gicheva, B. H. Bochev, C. D. Dushkin, and E. Adachi, "The effects of temperature and carboxylic acid ligand on the growth of nanocrystalline CdSe in a hot paraffin matrix," *Colloids and Surfaces A: Physicochemical and Engineering Aspects*, vol. 273, no. 1-3, pp. 10–15, 2006.

[36] S. Sapra, A. L. Rogach, and J. Feldmann, "Phosphine-free synthesis of monodisperse CdSe nanocrystals in olive oil," *Journal of Materials Chemistry*, vol. 16, no. 33, p. 3391, 2006.

[37] J. Jia, J. Tian, W. Mi et al., "Growth kinetics of CdSe nanocrystals synthesized in liquid paraffin via one-pot method," *Journal of Nano Research*, vol. 15, no. 6, 2013.

[38] H. Zhang and J. F. Banfield, "Identification and growth mechanism of ZnS nanoparticles with mixed cubic and hexagonal stacking," *Journal of Physical Chemistry C*, vol. 113, no. 22, pp. 9681–9687, 2009.

[39] N. T. K. Thanh, N. Maclean, and S. Mahiddine, "Mechanisms of nucleation and growth of nanoparticles in solution," *Chemistry Review*, vol. 3, no. 1, 2013.

[40] F. Huang, H. Zhang, and J. F. Banfield, "The role of oriented attachment crystal growth in hydrothermal coarsening of nanocrystalline ZnS," *Journal of Physical Chemistry B*, vol. 107, no. 38, pp. 10470–10475, 2003.

[41] C. L. Kuo, C. L. Wang, H. H. Ko et al., "Synthesis of zinc oxide nanocrystalline powders for cosmetic applications," *Ceramics International*, vol. 36, no. 2, pp. 693–698, 2010.